ments of volcanos with accuracy down to pixel is within the 800–900-m range. The smallest terrestrial shield edifice formed by one eruption also has a basal diameter of about 800–900 m [3].

The different types of volcanos can often be observed within the similar volcanic cluster on Earth. There are a variety of volcanic structures in similar clusters of volcanos in Saudi Arabia. The volcanic cluster and volcanos have been described in detail by Camp and Roobol [4]. The scoria cones are 0.5 to 1.3 km in diameter and rise as much as 100 m above the surrounding surface. They are typically steep and have open craters with a diameter of 100–400 m. Scoria cones are the largest group of Arabian volcanos with numbers up to 75% [4]. The shield volcanos are 5–10 km in diameter and rise as much as 1150 m above the surrounding surface. The crater/cone ratio is smaller, which is typical for shield volcanos. This group reaches 12% of the total number of volcanos [4].

References: [1] Sinilo V. P. and Slyuta E. N. (1989) *LPSC XX*, 1016–1017. [2] Frey H. and Jarosewich M. (1982) *JGR*, *87*, 9867–9879. [3] Macdonald G. A. (1972) *Volcanoes*, Prentice–Hall, New Jersey. [4] Camp V. E. et al. (1991) *GSA Bull.*, *103*, 363–391.

N93-14379

CONSTRAINTS ON CRUSTAL RHEOLOGY AND AGE OF DEFORMATION FROM MODELS OF GRAVITATIONAL SPREADING IN ISHTAR TERRA, VENUS.

Suzanne E. Smrekar and Sean C. Solomon, Department of Earth, Atmospheric, and Planetary Sciences, Massachusetts Institute of Technology, Cambridge MA 02139, USA.

Introduction: Gravitational spreading is expected to lead to rapid relaxation of high relief due to the high surface temperature and associated weak crust on Venus [1,2]. In this study, we use new Magellan radar and altimetry data to determine the extent of gravitational relaxation in Ishtar Terra, which contains the highest relief on Venus as well as areas of extremely high topographic slope. Within Ishtar Terra the only mountain belts found on Venus, Akna, Danu, Freyja, and Maxwell Montes, nearly encircle the smooth, high (3–4 km) plateau of Lakshmi Planum. Finite-element models of this process give expected timescales for relaxation of relief and failure at the surface. From these modeling results we attempt to constrain the strength of the crust and timescales of deformation in Ishtar Terra. Below we discuss observational evidence for gravitational spreading in Ishtar Terra, results from the finite-element modeling, independent age constraints, and implications for the rheology and timing of deformation.

Observations: Magellan data have revealed abundant evidence for localized extension throughout Ishtar Terra [3,4]. Many of the observed extensional features are oriented perpendicular to the downslope direction, implying that they formed as a result of gravitational spreading. In some of the mountainous areas, extensional faults occur parallel to the apparent direction of shortening. By analogy with the Himalayas on Earth [5], we interpret such extension to indicate gravitational spreading during convergence. Areas of possible gravitational spreading are observed in each of the four mountain belts and along both the southern and northeastern margins of Lakshmi Planum. Horizontal strain in these regions is estimated to be 1–20%; this value may be an underestimate if blocks are rotated along the normal faults. The observational evidence for gravitational spreading in Ishtar Terra is discussed more fully in [4].

Models: We use the finite-element algorithm TECTON [6] to model the evolution of gravitational spreading in a vertical section of the crust near the margin of a plateau or the edge of a broad mountain belt. Each model includes an elevated plateau 50 km in width, a sloped margin, and a lowlands region 80 km in width. The code employs a depth-dependent, viscoelastic rheology with nonlinear stress dependence and exponential temperature dependence. We adopt a Young's modulus of 6×10^{10} Pa, a Poisson's ratio of 0.25, and a diabase flow law [7]. Although a diabase composition is most similar to the composition determined at Soviet lander sites [8], the flow law determined for diabase may underestimate the strength because of partial melting of samples during the experiment [7,9]. For this reason, we also employ a websterite flow law [10] as an approximate upper bound on crustal strength. The surface temperature is 740 K and increases linearly with depth. Each row of elements in the grid has the same viscosity, which is equivalent to assuming that the temperature is constant along both the bottom and top of the grid. This results in a somewhat higher thermal gradient in the plains than in the plateau. The boundary conditions are zero vertical and horizontal velocity on the bottom of the grid, a free surface top boundary, and zero horizontal velocity and free vertical slip at the sides. The bottom boundary condition approximates an upper mantle layer that is much stronger than the lower crust. Details of the models are given in [4]. Brittle failure is evaluated using a Mohr-Coulomb criterion. The timing of predicted brittle failure and relaxation of relief are found for ranges of plateau height (1–5 km), plateau margin slope (1°–30°), crustal thickness (10–30 km), and thermal gradient (5–25 K/km). Slopes of 1°–30° and plateau or mountain belt heights of 1–6 km are observed in Ishtar Terra. Crustal thickness on Venus is predicted to be 10–30 km [11,12]; the average thermal gradient is expected to be 10–25 K/km [13,14].

The rate of deformation is largely controlled by the effective viscosity, and thus the temperature and stress, at the base of the crust. The greatest deformation occurs at the base of the crust, where the viscosity is lowest. Temperature at the base of the crust increases with crustal thickness (for a fixed thermal gradient), and deviatoric stress near the base of the crust increases with both crustal thickness and plateau elevation. The nonlinear change in predicted failure and relaxation time (see below) is due both to the exponential dependence on temperature and to the power law dependence on deviatoric stress of the effective viscosity.

Failure is predicted to occur when the stresses exceed the Mohr-Coulomb criterion. The earliest failure is located on the plateau. In most cases, failure on the slope follows shortly after failure on the plateau; thrust faulting in the plains is predicted typically only for a crustal thickness of 30 km. Figure 1 shows the time from the start of spreading until the first failure on the plateau as a function of plateau height and crustal thickness, for a margin slope of 3° and a thermal gradient of 15 K/km. Models with both websterite and diabase flow laws are plotted. No times are shown for models that do not fail within 1 Ga. Cases with a diabase rheology, a large plateau height, and a large crustal thickness fail almost immediately. A plateau height of 1 km and a crustal thicknesses of 10 km can take up to tens of millions of years to fail. With a websterite flow law, no failure occurs unless the crust is a least 20 km thick and the plateau elevation is 1–3 km. Changing the thermal gradient by 10 K/km has a large effect on failure times, with a higher thermal gradient decreasing the failure time by a factor of 10^2–10^4, and a lower thermal gradient increasing times by a similar factor. When failure is first predicted, the horizontal surface strain is approximately 0.05%. This strain is unlikely to be recognized as normal faulting in Magellan radar images; a strain of 1%, which accumulates once significant relaxation of the topography begins, is probably a more reasonable value to compare with observations. As faulting is not explicitly modeled, there is some uncertainty in the interpretation of

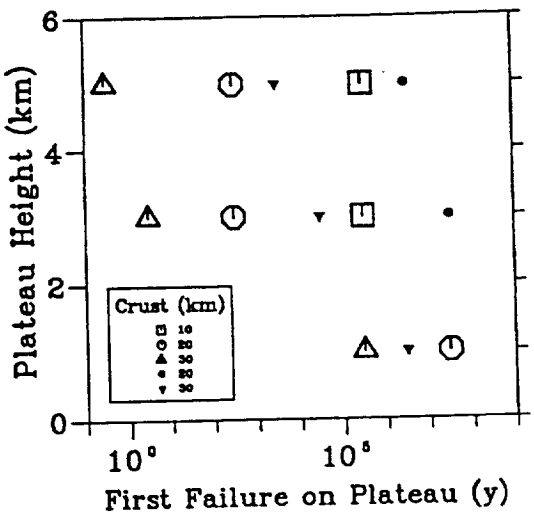

Fig. 1. The time at which failure (by normal faulting) first occurs on the plateau as a function of plateau elevation for three values of plains crustal thickness. The initial slope of the scarp in each model is 3°, and the plains thermal gradient is 15 K/km. Open symbols represent models with a diabase flow law [7]; filled symbols are for a websterite flow law [10]. Times are determined to the nearest order of magnitude.

strain after the initial failure. The total strain may be underestimated. As elevations in Ishtar Terra are among the highest on Venus, we assume that relief has not relaxed by more than 25% of its original value. The time at which the average elevation in the plateau has relaxed by at least 25% is shown as a function of plateau height and crustal thickness, for thermal gradients of 15 and 25 K/km, in Fig. 2. For a given thermal gradient and crustal thickness, predicted relaxation times for plateau heights of 1, 3, and 5 km vary by a factor of 10 at most. A 10-km change in crustal thickness leads to a factor of 10–100 change in relaxation time. Larger differences in relaxation time are predicted for models with the same plateau height and crustal thickness but with thermal gradients that differ by

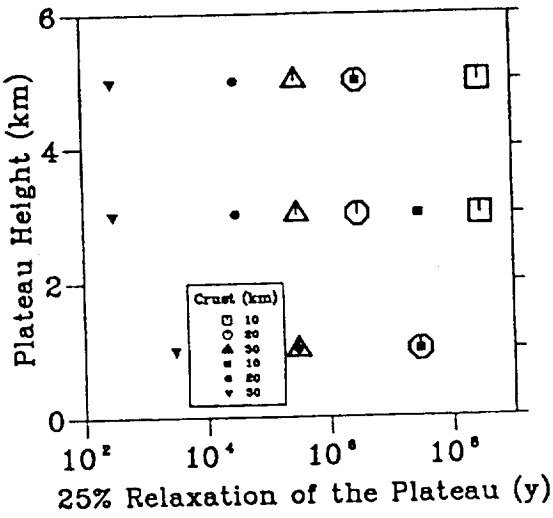

Fig. 2. The time at which the height of the plateau has relaxed by at least 25% as a function of plateau height for three values of plains crustal thickness. The initial slope of the bounding scarp is 3° and the flow law is that for diabase [7]. The open symbols are for a plains thermal gradient of 15 K/km; filled symbols are for a thermal gradient of 25 K/km. Times are determined to the nearest order of magnitude.

10 K/km, as is consistent with the larger changes in basal temperature. For a thermal gradient of 25 K/km and a plateau height of 1–5 km, all the models are predicted to relax by at least 25% within 100 m.y. for a 10-km-thick crust, 0.1 m.y. for a 20-km-thick crust, and 1000 yr for a 30-km-thick crust. A thermal gradient of 15 K/km gives relaxation times of up to 1 G.y., 100 m.y., and 0.1 m.y. for crustal thicknesses of 10, 20, and 30 km, respectively.

Discussion: The range of parameters can be narrowed somewhat by considering the geology and morphology of Ishtar Terra. In areas of possible gravitational spreading, the local topographic slope ranges from 2°–15°. For the purposes of discussion, we will assume a slope of at least 3°. Typical local relief is 2–3 km, although relief is as large as 5–6 km in Maxwell Montes. Thus models with plateau elevations of only 1 km can be eliminated as not relevant, especially given that the elevation may have relaxed somewhat from its original value. The very steep topographic slopes in many parts of Ishtar Terra suggest that the crust has been tectonically thickened and thus the topography is likely to be at least partially isostatically compensated. As mountains in Ishtar Terra rise 4–10 km above the surrounding lowlands, the crustal thickness is probably greater than 10 km. Further, the abundance of volcanism in Ishtar Terra, as well as the overlap of volcanism and extension in many areas [4], implies that the thermal gradient is unlikely to anomalously low. Values of 15 K/km or more are probably applicable. Using these limits on the ranges of parameters appropriate for Ishtar Terra and assuming a diabase flow law constrains relaxation of the topography by 25% to occur within 10 m.y. This result implies that either the crust is anomalous in some way—thinner, colder, or stronger than expected—or that mountain-building processes have maintained the relief in Ishtar Terra until geologically recent times. Independent information on the age of tectonism in Ishtar Terra is necessary to discriminate between these two hypotheses.

Information on the age of Ishtar Terra is inconsistent. The only available measure of absolute age, the average crater retention age for Venus of 500 m.y., implies that much of the surface is quite old [15]. Local geological information must be used to determine whether a region is likely to be older or younger than the average age [15]. In Ishtar Terra, the abundance of volcanism, especially in Lakshmi Planum, suggests that the surface may be less than the average age [16]. In many areas, both the shortening in the mountain belts and episodes of extension postdate local volcanism in Lakshmi Planum [3,4,16]. At least one impact crater in Ishtar Terra appears to be modified by extension due to gravitational relaxation [4]. However, Cleopatra, a 100-km-diameter crater, lies near the crest of Maxwell Montes and appears undeformed [17]. In addition to surface processes, gravity data suggest that dynamic processes in the mantle are actively supporting the long wavelength topography [18]. These dynamic processes may produce stresses capable of inducing the observed short-wavelength, high-amplitude variations in topography.

Both the gravity data and the majority of the geologic indicators favor the hypothesis that the region is likely to be younger than the average crater retention age of Venus, 500 m.y. On the basis of this information and the assumptions discussed above regarding the appropriate parameter range for Ishtar Terra, we interpret the results of our modeling to indicate that tectonic processes have maintained the topographic relief and high slopes of the region until as recently as 10 m.y. and may still be active.

References: [1] Weertman J. (1979) *PEPI, 19,* 197–297. [2] Smrekar S. E. and Phillips R. J. (1988) *GRL, 15,* 693–696. [3] Solomon S. C. et al. (1991) *Science, 252,* 297–312. [4] Smrekar S. E. and Solomon S. C. (1992) *JGR,* in press. [5] Armijo R. et al.

(1986) *JGR, 91,* 13803–13872. [6] Melosh H. J. and Rafesky A. (1980) *Geophys. J. R. Astron. Soc., 60,* 333–354. [7] Caristan Y. (1982) *JGR, 87,* 6781–6790. [8] Surkov Yu. A. et al. (1987) *Proc. LPSC 17th,* in *JGR, 92,* E537–E540. [9] Evans B. et al. (1990) *Geophys. Mono., 56,* 20 AGU. [10] Lallement H. G. Ave. (1978) *Tectonophysics, 48,* 1–27. [11] Grimm R. E. and Solomon S. C. (1988) *JGR, 93,* 11911–11929. [12] Zuber M. T. and Parmentier E. M. (1990) *Icarus, 85,* 290–308. [13] Kaula W. M. and Phillips J. R. (1981) *GRL, 8,* 1187–1190. [14] Solomon S. C. and Head J. W. (1982) *JGR, 87,* 9236–9246. [15] Phillips R. J. et al. (1992) *JGR,* in press. [16] Roberts K. M. and Head J. W. (1990) *Earth Moon Planets, 50/51,* 193–250. [17] Kaula W. et al. (1992) *JGR,* in press. [18] Grimm R. E. and Phillips R. J. (1991) *JGR, 96,* 8305–8324.

N93-14380

MULTIRESOLUTION PATTERN RECOGNITION OF SMALL VOLCANOS IN MAGELLAN DATA.

P. Smyth[1], C. H. Anderson[1], J. C. Aubele[2], and L. S. Crumpler[2], [1]Jet Propulsion Laboratory 238-420, California Institute of Technology, 4800 Oak Grove Drive, Pasadena CA 91109, USA, [2]Department of Geological Sciences, Brown University, Providence RI 02912, USA.

Introduction: The Magellan data is a treasure-trove for scientific analysis of venusian geology, providing far more detail than was previously available from Pioneer Venus, Venera 15/16, or ground-based radar observations [1]. However, at this point, planetary scientists are being overwhelmed by the sheer quantities of data collected—data analysis technology has not kept pace with our ability to collect and store it. In particular, "small-shield" volcanos (less than 20 km in diameter) are the most abundant visible geologic feature on the planet [2].

It is estimated, based on extrapolating from previous studies and knowledge of the underlying geologic processes, that there should be on the order of 10^5 to 10^6 of these volcanos visible in the Magellan data [3,4]. Identifying and studying these volcanos is fundamental to a proper understanding of the geologic evolution of Venus. However, locating and parameterizing them in a manual manner is very time-consuming. Hence, we have undertaken the development of techniques to partially automate this task. The goal is not the unrealistic one of total automation, but rather the development of a useful tool to aid the project scientists. The primary constraints for this particular problem are (1) the method must be reasonably robust and (2) the method must be reasonably fast. Unlike most geological features, the small volcanos of Venus can be ascribed to a basic process that produces features with a short list of readily defined characteristics differing significantly from other surface features on Venus [2]. For pattern recognition purposes the relevant criteria include (1) a circular planimetric outline, (2) known diameter frequency distribution from preliminary studies, (3) a limited number of basic morphological shapes, and (4) the common occurrence of a single, circular summit pit at the center of the edifice.

Pattern Recognition of Natural Objects: There has been little prior work on detecting naturally occurring objects in remotely sensed SAR images. Methods such as direct edge detection and Hough transform approaches deal poorly with the variability and speckle noise present in typical SAR imagery [5,6,7]. One approach toward detecting small volcanos is to use a template-matching method whereby a template of the object of interest is compared with the original target image by scanning the template over the entire scene. For an $N \times N$ square image and a $k \times k$ size template this operation takes the order of N^2k^2 operations. If scale-invariance is sought then typically the procedure is repeated using a range of template sizes. Wiles and Forshaw [8] have obtained promising results using this method despite the fact that the Magellan data contains significant speckle noise and ambiguity in terms of the appearance of volcanos in the imagery.

We have pursued an alternative approach motivated by the desire to develop real-time search methods that could be used as an interactive software tool by a planetary scientist. The key concept behind our approach is to carry out the detailed pattern matching at the lowest image resolution possible and to focus attention only on relevant parts of the image. Although our work is focused on developing useful image analysis tools rather than biologically plausible visual models, it is interesting to note that this general approach is consistent with high-level models of primate visual systems [9].

Multiresolution Pattern Recognition: The multiresolution paradigm emphasizes the decomposition of an image into a sequence of spatial band-pass components [10]. In this manner, image analysis can occur across various spatial frequencies while still retaining local spatial structure. The basic process is a series of recursive low-pass Gaussian decompositions of the original image, which in turn produces a bandpass Laplacian pyramid (the difference of Gaussians). From a pattern recognition standpoint the key feature of the method is the ability to analyze the image only at the coarsest scale necessary. For pattern matching the computational savings are significant, order of 4^k by working at the kth level of decomposition [11]. Furthermore, provided sufficient detail is retained for discrimination; by reducing the effective resolution of the image the input dimensionality to the detector also decreases by a factor of 4^k. The lower dimensionality makes it much easier to train an accurate detector. Focus of attention is implemented by simply "binning" the pixel values of the Laplacian components and then thresholding. Figure 1 contains an example of this process (note that a significant number of linear features are automatically omitted by focusing attention at the appropriate scale).

Volcano Discrimination: The focus of attention mechanism typically produces about 100 regions of interest (ROIs) per Laplacian image, roughly half of which contain volcanos and the other half primarily ridge or graben segments. Each ROI is labeled and a standard pattern recognition method (a neural network feed-forward classifier using backpropagation) is trained on samples of 5×5 windows of pixel values surrounding the detected bright spots. In our experiments with Magellan data the multiresolution filtering and focusing typically reduces the number of pixels that must be examined to order of 0.5% of those in the original image with a resultant speed-up in computation at the pattern-matching level. Using separate test and training images, roughly 70% mean ROI classification accuracy was attained (up from 50% by simply guessing).

The concept of having "ground truth" classification labels is actually incorrect since there are a significant proportion of ROIs whose labelings are not certain. Hence, by using subjectively estimated probability vectors of class labels (rather than deterministic class-label vectors of 0s and 1s) the mean ROI classification rate improved to about 82%. This probabilistic training method is consistent in terms of modeling posterior probabilities and, furthermore, will produce better posterior estimates than using "hard-decision" class labels given a finite amount of training data [12]. The mean missed detection and false alarm rates were about equal (roughly 20%)—almost all the incorrect decisions were made on windows where local context was not sufficient for accurate discrimination.